Department of Physics
Durham University

Fakultät für Physik und Astronomie
Ruprecht-Karls-Universität Heidelberg

On the evolution of dark matter haloes in quintessential dark energy models and possible effects on galaxy formation

Report on Level 4 Project

Tim Tugendhat

born in Ulm (Germany)

submitted in

April 2012

On the evolution of dark matter haloes in quintessential dark energy models and possible effects on galaxy formation

abstract:

In order to expand the GALFORM monte carlo merger tree code to quintessence models, it is vital to test whether the changes to the code suggested by Parkinson et al. (2008) are as accurate in quintessence as they are in ΛCDM. This will be done by comparing the trees to two previously conducted high-resolution N-body simulations. In this work, the quintessence models will be limited to those whose DE equation of state $w = p/\rho$ can be described by the Corasaniti-Copeland-Parametrisation (Corasaniti & Copeland, 2003). However, in principle, this can later be expanded to arbitrary $w(a)$.

We expect the galaxy formation to change mainly due to different initial power spectra $P(k)$, expansion histories, and different sets best-fit parameters for those cosmologies (as discussed in Jennings et al. (2010)). These effects all manifest themselves in the growth function $D(a)$, and the density contrast δ that is used to quantitavely describe structure formation and sets the seeds for galaxy formation.

Once reasonable agreement of the results of the merger tree algorithm for quintessence models are established, it would be most interesting to study how those models change galaxy formation with respect to ΛCDM, and what changes have to be made to GALFORM's initial parameters, and in what way they restrict the parameter space by comparing to observations.

This project was carried out by Tim Tugendhat at the

Institute for Computational Cosmology in Durham

under the supervision of

Prof Carlton Baugh

"All difficult things have their origin in that which is easy,
and great things in that which is small."
–Laozi
(Tao Te Ching chapter 63)

Contents

1. Introduction

1.1. Motivation

As the 2011 Nobel Prize in physics was awarded to three observational cosmologists "for the discovery of the accelerating expansion of the Universe through observations of distant supernovae"[*], we are once again reminded that much of the relatively young field of physical cosmology is still *terra incognita* on the map of fundamental research in physics. There have been ground–breaking discoveries in the last 20 years, among them the determination of cosmological parameters defined by models like ΛCDM within tight bounds, which is hailed as the beginning of an era of *precision cosmology*. We might as well use this new precision to go back to the drawing board and see if ΛCDM is not maybe a simplistic view of the universe. A varying Dark Energy ('Quintessence') or warm Dark Matter (WDM) are among those ideas.

However, some discoveries raise more questions than they answer. Now that we think that roughly 73% of the cosmos' energy density is made up of Dark Energy, we would very much like to know what it actually is and where it came from. The same goes for the no less mysterious Dark Matter, making up about 23%. The rest, a meagre 4% or so is no less than all the things that occupied scientists and scholars for the last couple of centuries: Galaxies, stars, planets, moons, space stations, humans, atoms, elementary particles, and light itself. The things we can see around us are literally the tip of the iceberg.

To figure out the reasons and mechanisms behind this cosmic balance that was able to spawn life to ask those questions in the first place is one of the main goals of physical cosmology. There are obviously big overlaps with other fields, such as particle physics, spawning new, exciting fields like astroparticle physics.

As we know very little about Dark Energy, apart from the fact that it is currently accelerating the expansion of the universe, there is a lot of speculation about its nature and origin. The arguably easiest way to account for it, is to give Einstein's "cosmological constant" Λ (Einstein, 1917) another chance. Or maybe leave some degrees of freedom and assume dynamical Dark Energy. This substance varies its *equation of state* ($w = p/\rho$) over time. There are also attempts to couple Dark Energy and Dark Matter; and, of course, to alter the laws of Einsteinian gravity.

The appeals of having a dynamical Dark Energy are obvious: Firstly, we have no reason why we should limit Λ to be constant over time. While this approximation is in very good agreement with observations, we cannot justify it physically. Apart from that, it would be a beautiful simplification to wed today's Dark Energy with models for Inflation in the very early universe. To explain some of the cosmos' properties, such as its fine-tuned flatness and homogeneity, the idea of cosmic inflation came up in the early 1980's (Guth, 1981). According to this idea, the universe must have undergone accelerated expansion in its very infancy.

---

[*]http://www.nobelprize.org/nobel_prizes/physics/laureates/2011/

Since the mechanisms that drive spacetime to expand in an accelerated manner are the same, trying to unify them is a physicist's first instinctive reaction.

1.2. This Project

The goal of this project work is to find out whether a non-constant equation of state $w(a)$ of dark energy will visibly affect galaxy formation. If a strong enough correlation between the dark energy model and predicted galaxy properties is found, with upcoming high–redshift surveys, this can be a novel observable of dark energy and maybe favour some models over others.

This particular question has not been explored vigorously enough by other authors, since galaxy formation models are cutting–edge research, albeit fast converging towards highly sophisticated semi–analytical codes such as Durham's GALFORM (Cole et al. (2000), Benson et al. (2002), Benson et al. (2003), Baugh et al. (2005)). Also, a number of high-resolution N-body simulations would be needed, each with a different cosmology. However, fast and accurate monte-carlo implementations to deliver dark matter halo merger trees to post-hoc galaxy formation codes have recently been delivered, such as the MERGER-TREES algorithm that now comes with GALFORM (Cole et al., 2008) (and its next-order corrections, see (Parkinson et al., 2008)). With new high-z surveys coming up, the observational end of this gap is closing fast as well.

Previous authors, such as Wang et al. (2007) have argued that changing cosmological parameters does not visibly affect galaxy properties, at least at low redshift. This conclusion is more or less a byproduct of comparing WMAP1 and WMAP3 parameters and testing the predicted galaxy formation against the SDSS catalogue. It is noteworthy that three different parameter sets for the semi–analytical model was used, and only those closest to SDSS were kept – in other words, the change in parameters for the background cosmology delivered *different* predictions for the galaxy formation and its history for the same galaxy formation parameter set.

2. Theoretical Background

2.1. General Dark Energy

Starting from Einstein's field equations,

$$G_{\mu\nu} + \Lambda g_{\mu\nu} = 8\pi G T_{\mu\nu}, \tag{2.1}$$

where Einstein's 'biggest bluder', Λ, represents a force counteracting gravity, we assume a perfect fluid (i.e. $T_{\mu\nu} = (\rho + p)u_\mu u_\nu + pg_{\mu\nu}$), and obtain Friedmann's equations,

$$\left(\frac{\dot{a}}{a}\right)^2 := H^2 = \frac{8\pi G}{3}\rho \tag{2.2}$$

and

$$\frac{\ddot{a}}{a} = -\frac{4\pi G}{3}\rho(1 + 3w), \tag{2.3}$$

where the following parameters have been implied

$$w := \frac{p}{\rho} \quad \text{and} \quad H := \frac{\dot{a}}{a}. \tag{2.4}$$

w is called the equation of state and plays a vital role in this work.

Note that we assumed zero curvature and absorbed Λ into the total energy density ρ, which is mathematically equivalent of having an extra term $\propto \Lambda$. This means phyiscally that this repellent force is nothing else but a constituent of energy density in the universe. The two Friedmann equations can be combined to find the conservation equation

$$\dot{\rho} + 3H\rho(1 + w) = 0. \tag{2.5}$$

Solving eq. (2.2) for ρ gives what is conventionally called the critical density:

$$\rho_{crit} = \frac{3H^2}{8\pi G}. \tag{2.6}$$

It means that if $\rho_{mean} = \rho_{crit}$, then the universe has zero curvature (since we ignored the curvature term in the Friedmann equations). If we now introduce

$$\Omega_{tot} := \frac{\rho}{\rho_{crit}} \quad \text{and} \quad \Omega_k := -\frac{K}{a^2 H^2}, \tag{2.7}$$

we find $\Omega_{tot} + \Omega_k = 1$ by definition. The advantage is that we now distinguish between physical energy density and curvature contributions.

We can now start to categorise different species of matter. For ordinary matter, like baryons, but also the (cold) dark matter component have a negible kinetic energy compared to their rest

mass, which means they are pressureless: $p = 0 \rightarrow w = 0$.

For highly relativistic matter, like photons or neutrinos where $T \gg m$, we get $\rho = 3p$ (meaning $w = 1/3$) from statistical physics. Note that this holds for Bosons and Fermions.

The next logical question to ask is how those species react on the expansion of the universe. Assuming w to be constant, integrating eq. (2.5) gives

$$\rho \propto \exp\left(-3 \int_1^a \mathrm{d}\ln(a')(1 + w(a'))\right), \tag{2.8}$$

assuming $w = w(a)$. This becomes $\propto a^{-3(1+w)}$ if $w = const$. For a static Λ, we require $\rho = const.$, therefore by eq. (2.8), $w = -1$.

The energy density ρ is most often devided into different constituents. Hence, we also get a fractional contribution $\Omega_i := \rho_i/\rho_{crit}$ for each of them.

2.2. Dark Energy model used in this project

The Dark Energy equation of state parametrisation we will be using here is the Corasaniti-Copeland-Parametrisation (Corasaniti & Copeland, 2003). It has 4 parameters which describe the behaviour of the equation of state. For example, w_0 is the value that $w(a)$ takes at $a = 1$. All of the models used here are undergoing a phase transition at an earlier time, described by a_m, converging towards w_m for $a \rightarrow 0$. Δ_m quantifies the 'severity' of the transition.

$$w(a) = w_0 + (w_m - w_0) \times \frac{1 + \exp\left(\frac{a_m}{\Delta_m}\right)}{1 + \exp\left(-\frac{a-a_m}{\Delta_m}\right)} \times \frac{1 - \exp\left(-\frac{a-1}{\Delta_m}\right)}{1 - \exp\left(\frac{1}{\Delta_m}\right)} \tag{2.9}$$

The six models that will be investigated are identical with the ones from Jennings et al. (2010). We have to consider that the best-fit values for cosmological parameters such as H_0, Ω_m, Ω_b from observations will change if we change the equation of state parameter. Jennings et al. (2010) present a method based on Komatsu et al. (2009) to find the 'WMAP7' best-fit for the given DE model. Basically, it is assumed that the distance priors used by Komatsu et al. should stay the same, while H_0, Ω_m, and Ω_b are treated as free parameters. They are fitted to three independent datasets, minimising $\chi^2_{tot} = \chi^2_{WMAP7} + \chi^2_{BAO} + \chi^2_{SN}$. This should give consistent and reliable fits. Another assumption is a zero curvature space, as always throughout this work as well.

The distance priors mentioned are the decoupling redshift, $z*$, a ratio called the 'acoustic scale', l_A, and a ratio called the 'shift parameter', $R(z*)$. The BAO and SN datasets have similar parameters with different names, but the idea is the same: fitting known scales to the models so that they meet early boundary conditions. This also distinguishes our models somewhat, and we have to be careful to check which effects come from the change in expansion history

Model	w_0	w_m	a_m	Δ_m
INV1	-0.4	-0.27	0.18	0.5
INV2	-0.79	-0.67	0.29	0.4
SUGRA	-0.82	-0.18	0.1	0.7
2EXP	-1.0	0.01	0.19	0.043
AS	-0.96	-0.01	0.53	0.13
CNR	-1.0	0.1	0.15	0.016

Table 1: The parameters used for eq. (2.9) in order to reproduce different models of Dark Energy. The INVs are inverse power–law potentials, SUGRA and CNR are tracking fields (i.e. Ω_ϕ is catching up with Ω_M), while 2EXP and AS are scaling solutions (i.e. the field behaves like a cosmological constant at late times).

Model	H_0	$\Omega_{m,0}$	$\Omega_{b,0}$
Millennium	73	0.25	0.045
ΛCDM	70.50 ± 1.3	0.2732 ± 0.006	0.046 ± 0.0008
wCDM	69.70 ± 1.4	0.2781 ± 0.009	0.047 ± 0.0009
Sanchez	71.50 ± 1.1	0.2610 ± 0.005	0.044 ± 0.0007
INV1	63.13 ± 0.5	0.2886 ± 0.022	0.095 ± 0.0023
INV2	68.21 ± 0.7	0.2666 ± 0.011	0.051 ± 0.0014
SUGRA	67.63 ± 0.7	0.2427 ± 0.014	0.059 ± 0.0016
2EXP	70.01 ± 0.8	0.2816 ± 0.005	0.045 ± 0.0017
AS	70.42 ± 0.9	0.1734 ± 0.021	0.043 ± 0.0017
CNR	70.05 ± 1.2	0.2853 ± 0.022	0.426 ± 0.0026

Table 2: The best fit parameters as described above. The errors are 1σ. The values are overall roughly consistent with the concordance model of $\frac{1}{4}$ dust and $\frac{3}{4}$ Dark Energy with a Hubble parameter of somewhere around $70\frac{\text{km}}{\text{Mpc·s}}$. Included are also the values used for the MS, the 5-year best fit ΛCDM and wCDM. The tuple labelled 'Sanchez' is a cosmology used in one of the two large N-body simulations that had been carried out at the ICC, it derives its values (and name) from Sánchez et al. (2009). All are in flat space, so $\Omega_{DE,0} = 1 - \Omega_{m,0}$.

and which come from the change in the other cosmological parameters, such as $\Omega_{m,0}$. The best fit values given by Jennings et al. can be found in Table 2. Something that will be affected by the Dark Energy equation of state is doubtless the (normalised) growth factor $G = D/a$. How D is calculated in the linear regime can be seen in the appendix.

It follows (Linder & Jenkins, 2003)

$$G'' + \left(\frac{7}{2} - \frac{3}{2} \frac{w(a)}{1 + X(a)} \right) \frac{G'}{a} + \frac{3}{2} \frac{1 - w(a)}{1 + X(a)} \frac{G}{a^2} = 0, \tag{2.10}$$

with

$$X(a) = \frac{\Omega_m}{1 - \Omega_m} \exp\left(-3 \int_a^1 \mathrm{d}\ln a' \; w(a') \right).$$

So although the power spectra should be normalised to the same σ_R today, the history of stucture growth is expected to be different.
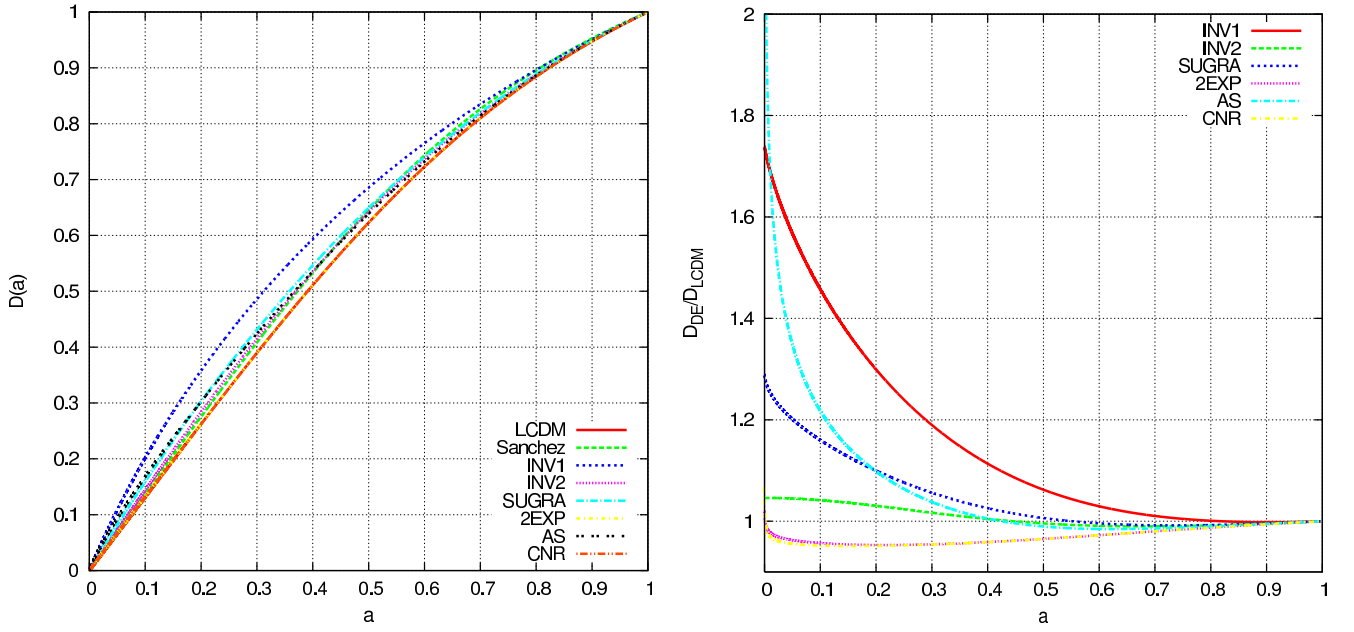
Figure 1: Left panel: $D(a)$ for the different cosmologies presented in table 1. They are all using the same H_0, $\Omega_{m,0}$, $\Omega_{b,0}$ (**Millennium** parameters). Yet, there are noticable differences. The function has been normalised so that $D(a_0) = 1$.
Right panel: $D_{DE}/D_{\Lambda\mathrm{CDM}}$, notice that big relative differences of $\sim 10\%$ already at $a = 0.5$, or $z = 1$.
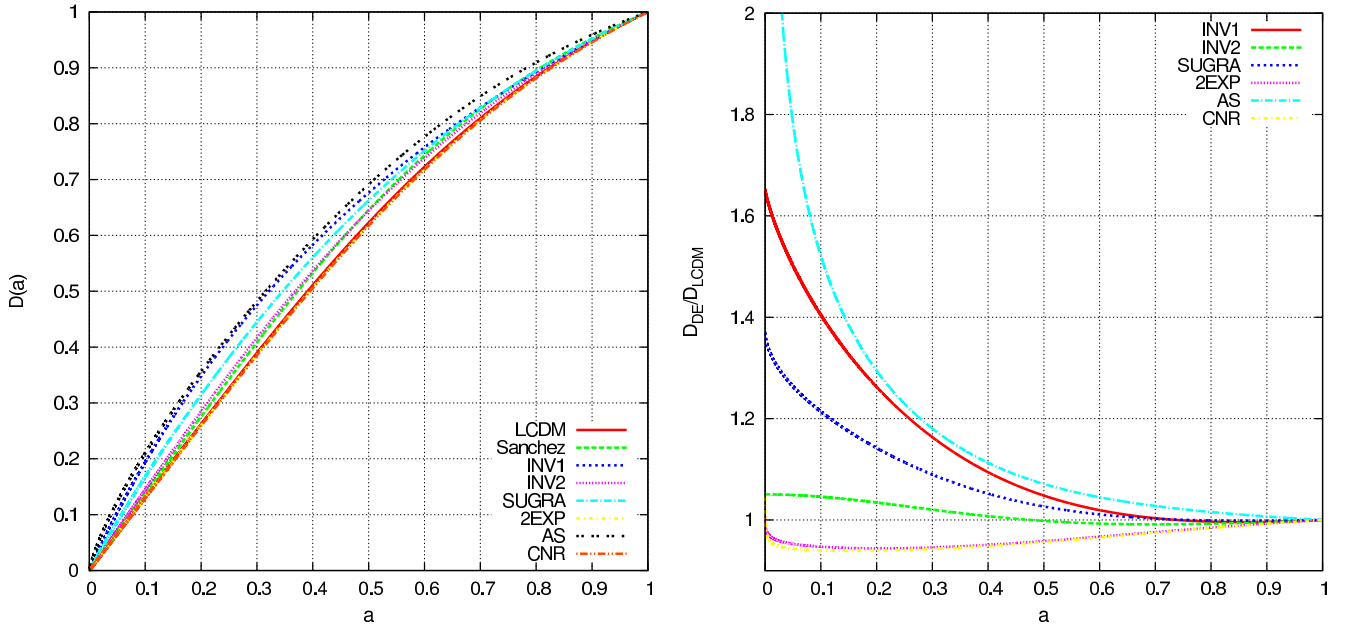
Figure 2: Left panel: $D(a)$ for the different cosmologies presented in table 1. This is the parameter set that uses the **best fit** for each model.
Right panel: $D_{DE}/D_{\Lambda\mathrm{CDM}}$, same as above. The differences remain as big; the history equation of state seems to play a vital role.
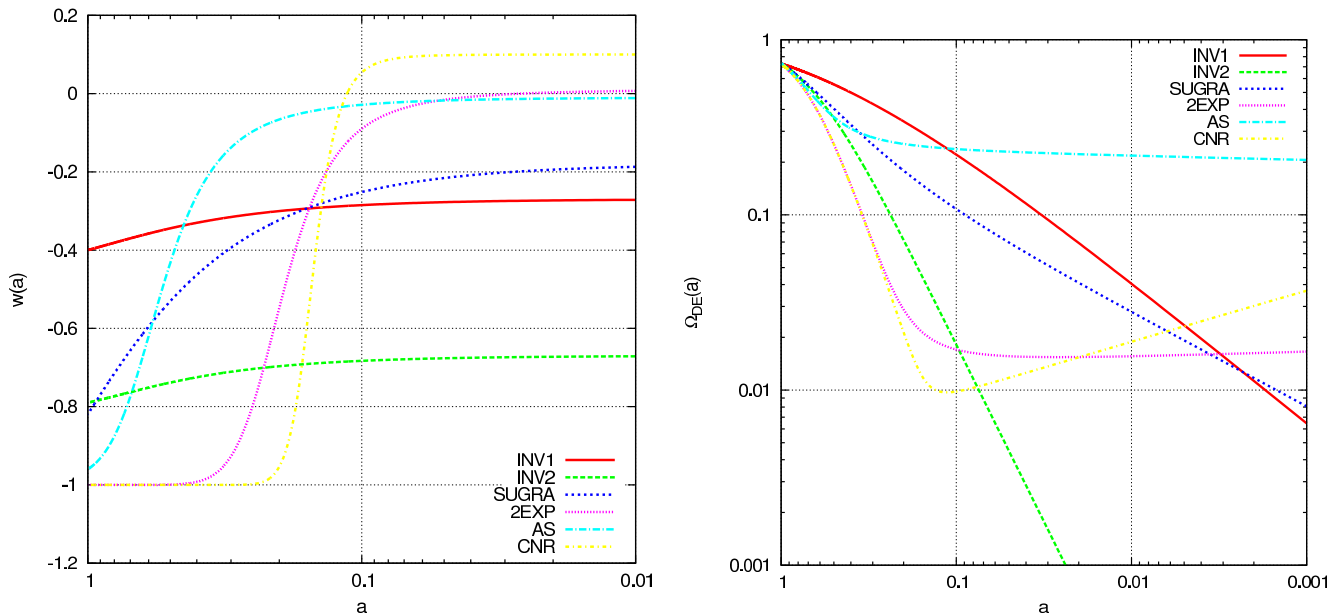
Figure 3: Left panel: $w(a)$ for the different cosmologies presented in table 1.
           Right panel: Ω_{de} for the associated equations of state.

2.3. Precision cosmology

As stated in the introductory remarks, there have been remarkable advances in physical cosmology in the last 20 years. We've come from a rough estimation of the age of the universe to a full and very precise cosmic inventory. The only problem is that we don't know what it is that makes up about 95% of what we're taking inventory of.

The discovery of the cosmic microwave background radiation (CMB or CMBR) (Penzias & Wilson (1965), Dicke et al. (1965)) was one of the biggest steps forward in this field. The predicted relic radiation from a hot big bang (which was by no means an accepted paradigm at this time), a near-perfect blackbody, which has now been redshifted to millimetre-wavelengths, spurred the research in cosmology.

There have been many observations of the CMB in the last 20 years, but by far the most precise and ground-breaking have been made by the *COBE* (Boggess et al., 1992) and *WMAP* (Bennett et al., 2003) satellites since the early 90's and the early 00's, respectively. The newest probe, *PLANCK*, which will measure the CMB to an unprecedented accuracy (Planck Science Team, 1996), has been operational for nearly 3 years, but results of cosmological importance have yet to be published. According to the ESA website, they can be expected in early 2013 (Planck Science Team, 2012). The most precise data that is publicly available is the 7–year WMAP data compiled by Komatsu et al. (2011).

The most remarkable thing about the data seen in table 3 are the comparatively small error bars. About a decade ago, these were one order of magnitude larger, and people argued vigorously whether H_0 is around 50 or 100 $\frac{\text{km}}{\text{s Mpc}}$.

Also, note that w is very close to -1. However, values < -1 are not excluded. This is a

special case called *phantom* energy. It has the disturbing property of giving the universe only a finite time to exist, before ending in a big rip. These models are –as of now– not subject of this project, but are, due to the high flexibility of the codes used (we will see this in the next section), not impossible to include.

2.4. Dark Matter Haloes

Our current understanding of galaxy formation is that each galaxy has a halo of dark matter around it, which extends much farther than the (visible) galaxy itself. These haloes are suspected to form hierarchically, i.e. from small to big scales. Lighter haloes are formed first, collapsing and merging into bigger and bigger ones as time goes on.

To track these mergers over time is vital to any galaxy formation model, since the galaxies are mere tracers of those haloes. Of course, individual development of galaxies also has to be considered and modelled carefully.

2.4.1. Spherical Collapse

In order to simplify the problem of structure formation, it is modeled as *spherical* halos collapsing. Since they mainly consist of dark matter, another assumption is collisionlessness of the particles. This does not mean that the collapse goes on forever; at some point, the halo will virialise, meaning an equilibrium† between potential and kinetic energy is reached. The density of the collapsed halo in terms of the critical denisity is called Δ_V. During matter-domination, the numerical value of this is ≈ 178.

To see what happens over time when a spherically symmetric (i.e. no angular derivatives, no shear, etc.) overdensity collapses, a Newtonian approach can be used.

Consider

$$\ddot{R} = -\frac{GM(R)}{R^2}, \tag{2.11}$$

which is the Newtonian law of gravity; a dot $\dot{}$ represents a total time derivative. If we insert a spherical mass distribution of constant mass, i.e.

$$M(r) = \frac{4\pi}{3}\rho r^3,$$

and remember that for dust the background density ρ_0 scales as a^{-3}, in particular

$$\rho_0 = \frac{3}{4\pi}M(R_0)(R_0 a(t))^{-3} = \rho\left(\frac{R}{R_0 a(t)}\right)^3,$$

---

†this is stable in a Einstein-deSitter Universe; if there is dark energy present, the equilibrium can be assumed to be stable temporarily
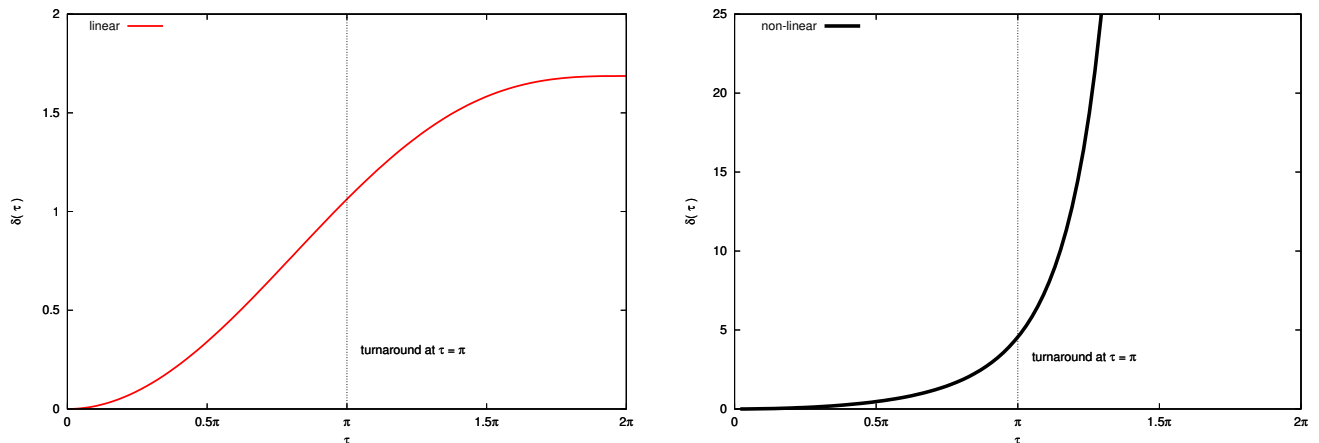
Figure 4: δ as a function of the parameter τ. The red line is the linearised function, the black line is the nonlinear version. The turnaround at $\tau = \pi$ is marked.

then we can write $\delta = (\rho_0/\rho) - 1$ as

$$\delta = \left(\frac{R}{R_0 a(t)}\right)^3 - 1. \tag{2.12}$$

Keep in mind that $\delta = 0$ outside, i.e. delta is a top-hat function. Multiplying both sides of Eq. 2.11 by $2\dot{R}$ and integrating once we obtain

$$\dot{R}^2 = 2\frac{GM}{R} - C. \tag{2.13}$$

This can be solved analytically, albeit parametrically in R-t-space if $C > 0$:

$$R = GMC^{-1}(1 - \cos(\tau)), \quad t = GMC^{-3/2}(\tau - \sin(\tau)), \quad \tau \in (0, 2\pi). \tag{2.14}$$

Putting in δ from above and keeping in mind that $a(t) \propto t^{2/3}$ during matter domination $(w_{eff} = 0)^{\ddagger}$, we end up with a function $\delta(\tau)$:

$$\delta(\tau) = \frac{9(\tau - \sin(\tau))^2}{2(1 - \cos(\tau))^3} - 1, \tag{2.15}$$

which reads, when linearised, according to (12.75) in Amendola & Tsujikawa (2010):

$$\delta_{lin}(\tau) = \frac{3}{5}\left(\frac{3}{4}(\tau - \sin(\tau))\right)^{2/3}. \tag{2.16}$$

The overall behaviour is as expected (see fig. 4): The sphere expands with background evolution, however, it decelerates, decouples more and more from the Hubble flow, until the turnaround, at $\tau = \pi$, and then collapses on itself, i.e. the density diverges. This is, interest-

---

‡From Eq. 2.2: $\dot{\rho}/\rho = -3\dot{a}/a \Rightarrow \rho \propto a^{-3}$, from Eq. 2.5: $\dot{a} \propto \sqrt{\rho}a \propto a^{-1/2} \Rightarrow a \propto t^{2/3}$

ingly enough, the same behaviour that a closed universe as a whole whould exhibit, according to Birkhoff's theorem.

The value of δ_{lin} at $\tau = 2\pi$ is called critical or collapse density, $\delta_{crit} \approx 1.686$, since density contrasts which reach this value in the linear regime, should have collapsed onto themselves.

As mentioned before, virialisation is thought to set it at $a \approx a_{coll}$. The density of the halo at this point is called virial overdensity Δ_V. The virial theorem states that if a force resulting from a potential energy that obeys $V(ar) = a^k V(r)$, then the kinetic energy T and the potential energy V are related by

$$T = \frac{r}{2}\frac{\partial V}{\partial r} = \frac{kV}{2}. \tag{2.17}$$

For gravity ($V \propto -R^{-1} \rightarrow k = -1$), this simplifies to $T = -V/2$.

Assuming energy conservation, we then find

$$V_{ta} = V_{vir} + T_{vir} = \frac{V_{vir}}{2}, \tag{2.18}$$

since at turnaround (subscript ta), kinetic energy vanishes and at virialisation (subscript vir) $T_{vir} = -V_{vir}/2$.

For a uniform sphere, $U(R) = -3GM/5R$; if $M = const.$, then we can infer that $R_{ta} = 2R_{vir}$. Therefore, the virialised density picks up a factor of $2^3 = 8$ with respect to the value at turnaround. Furthermore, in a matter-dominated universe, we have $\bar{\rho} \propto a^{-3} \propto (t^{-2/3})^3 = t^{-2}$. With $t_{vir} = 2t_{ta}$, we thus pick up another factor of $0.5^{-2} = 4$.

The final density is then

$$\Delta_V = 4 \times 8 \times (\delta_{ta} + 1). \tag{2.19}$$

Taking eq. at $\tau_{ta} = \pi$, we get

$$\Delta_V \approx 178. \tag{2.20}$$

This is the line between background matter fields and highly unlinear structure which we are interested in. It is being used in Press–Schechter theory (Press & Schechter (1974)). In an Einstein-de Sitter (EdS) universe (i.e. $\Omega_m = 1 \; \forall \; a$), this value is constant.

It changes, however, if Dark Energy is present. How to calculate the critical density contrast for a given Dark Energy was a challenge to be solved in this work.

2.4.2. Merger Trees

Simulations can only work with discrete time steps. Outputs are usually quite far apart ($\Delta z = \mathcal{O}(10 - 0.1)$), so the concept of merging haloes are becoming *merger trees*, where haloes can only be tracked at fixed and discrete times z_i. In N-body simulations, such as the Millennium Simulation (MS), this is usually done by identifying groups of particles (Friends of friends, FoF), and tracking them over the course of the simulation. Then, post-processing algorithms

are used to analyse these groups further, for example identifying 'false' haloes that have been linked by mistake because they have a residue overdensity of particles between them due to a previous interaction, but also for finding density peaks within the haloes, so-called sub-haloes (which are actually the haloes known from galaxy formation. Sub-halo and halo are often used synonymously, unfortunately adding some confusion for inexperienced readers). In the end, one should have a database of different merger trees, which can be used further for semi-analytic galaxy formation models (SAMs).

This method has one major flaw: it is based on N-body simulations, which are computationally expensive. Depending on size and resolution, a single run can take several days or even weeks on a medium-sized computing cluster.

A much quicker method is a monte-carlo approach which is only concerned with haloes and their statistical properties. Another positive aspect is that the resolution is finer than with N-body simulations. A downside of this is obviously that the haloes are not spatially resolved. However, many important other galaxy properties, such as luminosity functions, or the star-formation rate can be inferred. This is our method of choice here due to the many different models of Dark Energy used.

Figure 5: A sample merger tree. The size of a halo corresponds to its mass. A massive halo at redshift z_0 is the result of a merger of individual haloes between z_1 and z_0. The earlier we go, the more progenitors are found. This is the priciple of hierarchical structure formation.

2.5. The semi-analytical galaxy formation code galform

GALFORM is being actively developed at the ICC in Durham. The aim is to have an accurate semi-analytic code for galaxy formation in hierarchical cosmologies. An advantage of the code is that it can either take merger-trees from N-body simulations (which have spatial resolution) or generate its own trees with its own monte-carlo based algorithm. One of the aims of this project was to find out what it would take to re-write this algorithm so that it produced merger-trees for a given Dark Energy model (for now limited to models whose equation of state is parametrisable with Eq. 2.9).

The tree-forming algorithm, called MERGER-TREES, makes one tree at a time by randomly splitting base masses according to the power spectrum for each time step. Inputs needed are,

apart from the power spectrum, only the time-dependend critical overdensity, $\delta_{crit}(a)$ and the virial overdensity Δ_V. Both sets can be provided in simple ASCII files. Then, trees can be produced at given redshifts z_i, with base redshift z_0. The output has to be saved somehow, before calculating the next tree, as they use the same memory allocation. The code runs quite fast, but parallelisation could actually be implemented, because the trees are in principle generated completely independently.

3. Project work progress

First, we had to establish that MERGER-TREES delivers an as-good approximation to the 'true' merger trees as well in non-ΛCDM cosmologies; in order to do this, we have snapshots of a large ΛCDM simulation and a simulation with the SUGRA DE model, using the parameters labelled 'Sanchez' and 'SUGRA'[§] respectively in table 2 . Those have been carried out a while ago at the ICC, but fit our purposes well. One drawback is that the latest snapshot of both of them is at $z = 5$. Their box size is $L = 50(\text{Mpc}/h)^3$ and particle numbers are $N = 1024^3 \approx 10^9$, resulting in a particle mass of $M_p = 8.4 \cdot 10^6 M_\odot/h$ for 'Sanchez' and $M_p = 7.85 \cdot 10^6 M_\odot/h$ for SUGRA. In comparison, the MS had $L = 500(\text{Mpc}/h)^3$, $N = 2160^3 \approx 10^{10}$ and $M_p = 8.6 \cdot 10^8 M_\odot/h$. So the simulations we can use are better resolved than the MS. Assuming we establish agreement with both simulations, we might feel the need to establish whether the algorithm also fits well at lower redshifts.

In order to do so, we need to extract 'real' merger trees from the simulations and compare their properties (such as the mass function w.r.t. time, the conditional mass function w.r.t. halo masses and time, etc.) to the ones that the monte-carlo code generates.

Fortunately, the MERGER-TREES algorithm is easily altered to give merger trees in an arbitrary cosmology, as long as structure forms hierarchically. To achieve this, we had to provide the initial conditions, i.e. generate power spectra for the different cosmologies and – after a bit of alteration to the code – provide the (linearised) density contrast for which a sphere would collapse at time a, called $\delta_{crit}(a)$.

3.1. Calculating $\delta_{crit}(a)$, Δ_V for different DE cosmologies

Since MERGER-TREES requires a tabulated file for δ_{crit} and Δ_V, it was quite vital to accurately calculate them for all models. To obtain $\delta_{crit}(a)$, the nonlinear evolution equations have to be evaluated numerically for a big set of different initial conditions, since each run with one set of ICs gives us exactly one point of the graph of $\delta_{crit}(a)$.

This has been realised in Python, see A.2 for the complete code. It takes about an hour to run on a normal laptop computer and will produce the ASCII file that MERGER-TREES needs.

To see this, consider the non-linear evolution equation of the density contrast for nonrelativistic matter (CDM) in a spherical perturbation (for a derivation from the basic hydrodynamical equations, the reader is referred to Pace et al. (2010)),

$$\delta'' + \left(\frac{3}{a} + \frac{E'(a)}{E}\right)\delta' - \frac{4}{3}\frac{\delta'^2}{1+\delta} - \frac{3}{2}\frac{\Omega_{m,0}}{a^5 E^2(a)}\delta(\delta+1) = 0, \tag{3.1}$$

[§]Supergravity

and its linear counterpart,

$$\delta'' + \left(\frac{3}{a} + \frac{E'(a)}{E}\right)\delta' - \frac{3}{2}\frac{\Omega_{m,0}}{a^5 E^2(a)}\delta = 0. \tag{3.2}$$

The nonlinear equation above is, incidently, the same as Eq. (12.20) in Amendola & Tsujikawa (2010), the only difference being there, the authors are using the derivative w.r.t. $N = \ln(a)$, whereas we are using derivatives w.r.t. a, as it is – despite being aesthetically less pleasing – numerically much easier to implement.

The idea is to solve the non-linear equation 3.1 for given inital conditions (δ_0, δ_0'), starting from a small scale factor $a_{initial}$, which has chosen to be $a_{initial} = 10^{-4}$. This choice is due to numerical limitations. Much smaller initial scale factors will take much longer to solve the DEs, bigger scale factors will start affecting the precision at 'interesting' scale factors $a \sim 0.1...1$. The schematics can be seen in fig. 6.

Numerical tests have confirmed the findings of Pace et al. (2010), i.e. that the solution is almost independent of δ_0', so it has been hard-coded to be $\delta_0' = 5 \cdot 10^{-5}$. Also, since the nonlinear curve is very steep while diverging, the result is quite insensitive to the actual numerical choice of when we define the curve as 'diverged'. In this work, the chosen value was $\delta_{NL} \geq 5 \cdot 10^5$. To obtain a whole dataset of (a_d, δ_{crit}), we simply have to loop over the above mechanism, while evolving to ever smaller initial conditions δ_0. This has been implemented in the code. The only input now is the 'starting' initial condition δ_0 and the number of iterations N, together with the parameters of the w-parametrisation (table 1) and the three best-fit parameters for the cosmology from table 2.

For the virial overdensity Δ_V, we follow the recipe used by Pace et al. (2010). The idea is to determine the turnaround scale factor a_{ta} by solving the above nonlinear equation and finding the minimal value for $\log(1 + \delta)a^{-3} \propto 1/R$, thus maximising the sphere's radius.

We then only need to multiply $(\delta_{ta} + 1)$ – just as the analytical derivation in section 2.4.1 – by $y^{-3} = (R_{ta}/R_{vir})^3$ and $x^3 = (a_{vir}/a_{ta})^3$.

We can take $a_{vir} = a_{coll}$. For y, we take the equation for non-clustering dark energy derived by Maor & Lahav (2005). This is equation (26) in their paper and solve it for y:

$$-2y^3 x^{-3}q + (1 + q)y - \frac{1}{2} = 0 \tag{3.3}$$

Here, $q = \Omega_{DE,ta}/\Omega_{m,ta}$. If one takes the limit $q \to 0$ (meaning matter domination, or an EdS universe), then $y \to 1/2$, reproducing the result we had in section 2.4.1.
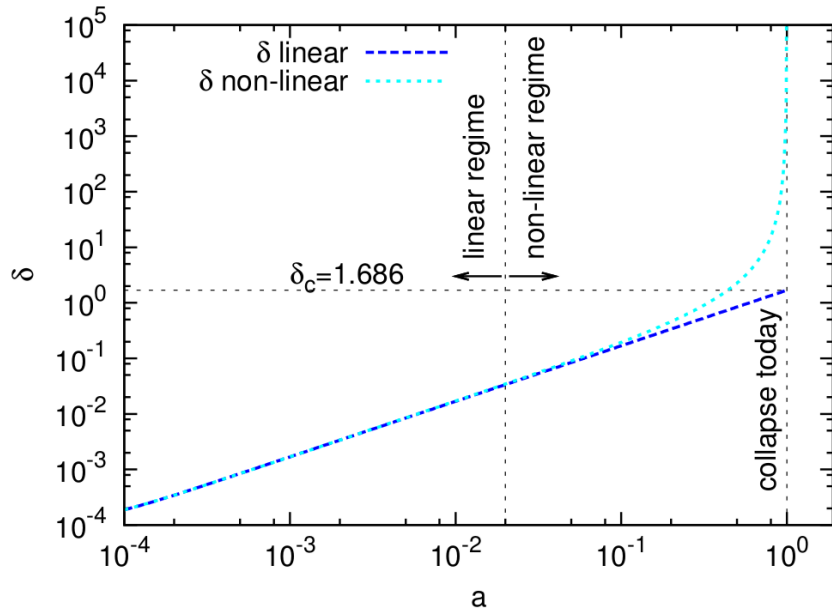
Figure 6: One iteration of the algorithm shown in fig. 7. This is fig. 1 directly taken out of Pace et al. (2010). Here, $a_d = 1$, and we are in an $\Omega_m = 1$ case, so $\delta_{crit} \approx 1.686$.
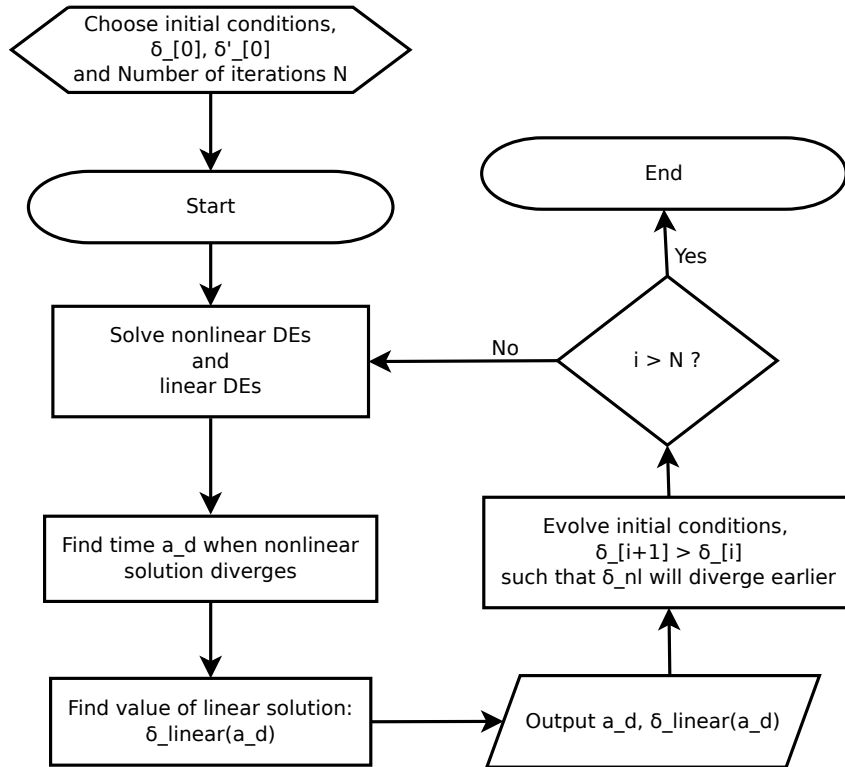
Figure 7: A flowchart illustrating the code that is calculating δ_{crit} for different cosmologies. The user inputs the inital conditions and the number of iterations, the code then calculates N times δ_{crit} with decreasing initial condition. If the first IC is chosen correctly to lie around $a_{coll} \approx 1$, then, for around $N \approx 50$, the output will span from $a_{coll} \sim 1.0...0.05$, spaced approximately logarithmically.
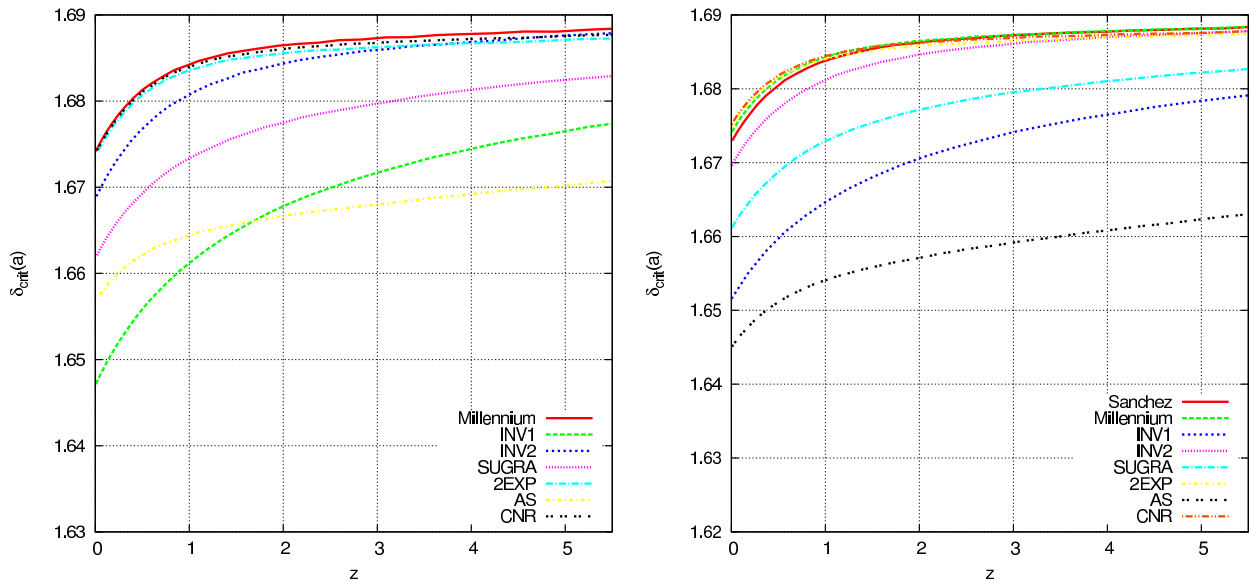
Figure 8: Even in such a subtle parameter as δ_{crit}, there are visible differences between the models. It is quite feasible that the differences will affect galaxy formation in one way or another. Whether or not these differences produce a strong enough signal to detect is still to be determined. Again, we have to make sure to distinguish between effects from the cosmological parameters and the ones inherent to the DE cosmologies. It will be difficult to distinguish between those once we're considering galaxy formation; there will be some degeneracies. **Left panel:** δ_{crit} for the cosmologies with the **Millennium** parameter set for H_0, Ω_m, Ω_b, **Right panel:** δ_{crit} for the cosmologies with their respective **best-fit** parameter set.

3.2. Power spectra

The first step here was to find a code that provides a power spectrum, a transfer function, and so on. There are some codes around, the most accomplished of which is probably CMBFAST. However, since it doesn't support a variable w, we decided to go with the CMBFAST-based CAMB (Lewis et al., 2000), which provides a neat addition to its original code by W. Fang (Fang et al., 2008) that allowes an arbitrary $w(a)$, by simply providing a tabulated ASCII file for it. This can easily be achieved by writing a script that calculates those for our given cosmologies (see tables 1 & 2). We were lucky enough to obtain the original data and code from Jennings et al. (2010), since the current, updated version of CAMB doesn't work with Fang's modifications. Since the code is the same, we get identical power spectra. We have to be careful about the parameter changes again. To illustrate the differences, fig. 9 shows the power spectra of our used cosmologies both with their own best-fit values and with ΛCDM concordance values. The power spectra used in our work are all normalised to $\sigma_8 = 0.8$ at $z = 0$ as observations require. In the plots, they are normalised to the CMB fluctuations due to the readability of the graph.
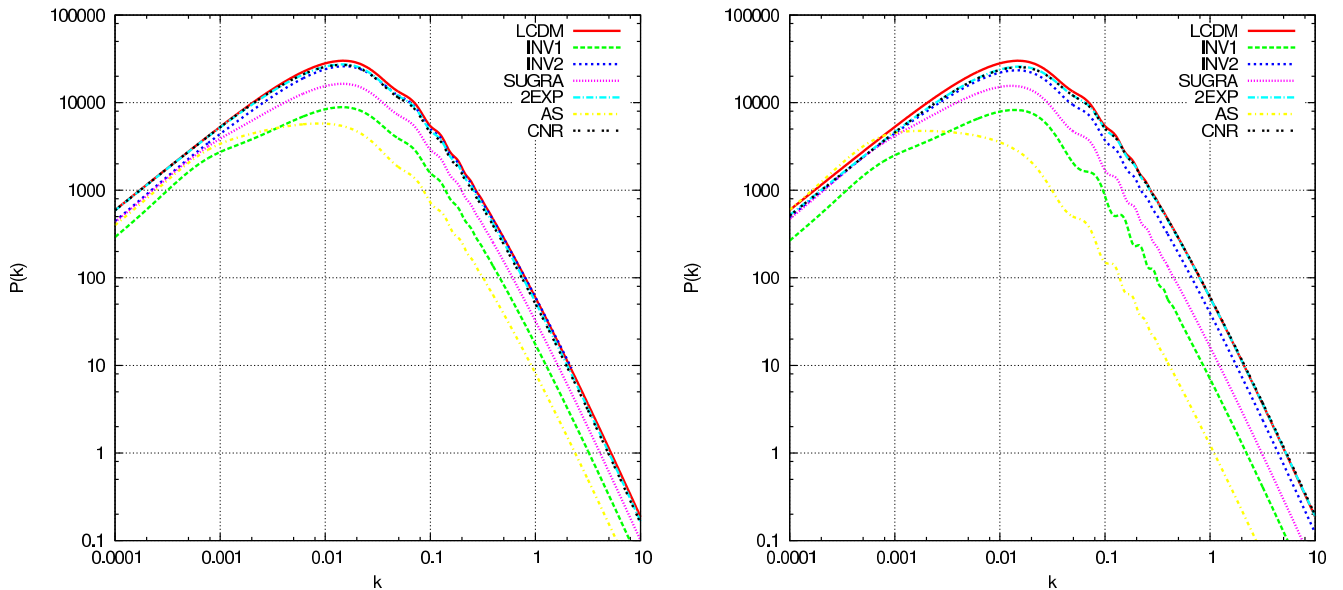
Figure 9: Left panel: $P(k)$ at $z = 0$ for the different cosmologies presented in table 1. They are all using the same H_0, $\Omega_{m,0}$, $\Omega_{b,0}$ (**Millennium**). There are obvious differences, expecially in the turnover position. They are normalised to have the same fluctuations (σ_8) at the recombination redshift. This way, they are further apart in this plot and the differences in shape can be seen. Also, the strength of the different Dark Energies on the fluctuations show themselves in the difference in amplitude.
Right panel: $P(k)$ at $z = 0$ for the different cosmologies presented in table 1, with their **best fit** values from table 2. The differences to the left panel are only subtle.

3.3. Conditional mass functions

After having adapted the Fortran code for MERGER-TREES to be able to read in the produced files for δ_{crit} instead of producing its own version of it, the given cosmologies can be theoretically produced by the code. To test this, we found two simulations which were done a while ago at the ICC, one for a 'Sanchez' and one for a 'SUGRA' cosmology. We decided to check if the conditional mass function, an indicator of halo splitting ratios, was still in as good agreement as in Parkinson et al. (2008), or if the adaptions of 'new trees' had to be looked at again. Also, the ΛCDM case of our version of the code should reproduce the results of the original code with the same cosmology.

The conditional mass function is the fraction of the final halo mass (M_2) that is in progenitors of mass M_1 per unit log bin in $\log M_1$ (see, for example, (Cole et al., 2008)).

The ones from Parkinson et al., which are done for ΛCDM (i.e. a 'Millennium' cosmology), have been successfully reproduced, see fig. 10. The apparent downside is that the 'custom' cosmology almost perfectly lines up with the ΛCDM case. This had to be investigated more closely. Obviously, the SUGRA cosmology here uses the best-fit parameters also used in the N-body simulation. So we have two different cosmologies lining up albeit having different parameters. If we produce a plot for a Sanchez cosmology, with only quite small changes w.r.t. the Millennium case, the differences become apparent (see fig. 11).

This is a part success of what we have been trying to find, i.e. that the equation of state $w(a)$ affects structure formation visibly. The problem in the first plot (fig. 10) is that the shifts in H_0 and Ω_0 end up compensating the different growth function (and thus δ_{crit}) and power spectrum. To compute the conditional mass functions, we have written another Python script. It takes – depening on the resolution – a couple of hours to run. For portability, the programme was written in a modular fashion, see again A.2.

3.4. Analysing the gadget–simulations

Fortunately, there are 2 GADGET-simulations on the storage at the ICC with identical parameters (boxsize, particle mass, etc.), except for the cosmologies. These were going to be our benchmark to see how well MERGER-TREES is dealing with different cosmologies. To do this however, we have to extract merger trees from the snapshots, which proved to be a complicated process. First, we need to run SUBFIND (Springel et al., 2001) on the snapshots to seperate friends-of-friends groups into subhaloes. These then in turn have to be linked over timesteps, and possibly extrapolated if at some timestep, a certain halo was not found by either FoF or subsequently SUBFIND. This is done by a set of Fortran programmes that John Helly provided; the runtime on a high performance computer such as cordelia in the ICC is on the order of 20 hours.

The outputs are binary files, which can be read in using yet another Python script (which heavily borrows functions from a Python script of John Helly's).

The conditional mass functions didn't quite look as expected. So, in order to troubleshoot, the first thing we did was see what the mass function at $z = 5$ (the latest output redshift) looked like for the simulations. The results were unexpected. There seems to be a plateau-like feature in the mass functions, which obviously isn't supposed to be there. Since the code works fine on simulations we know to be correct (e.g. the Millennium Simulation), we assume the simulations to be faulty. The outputs have not yet been used for anything, so we are the first ones to examine these particular simulations. What could be the reason for such an apparent failure to reproduce analytical fits to mass functions (such as Sheth & Tormen (2002)) will have to be subject to further inquiry.
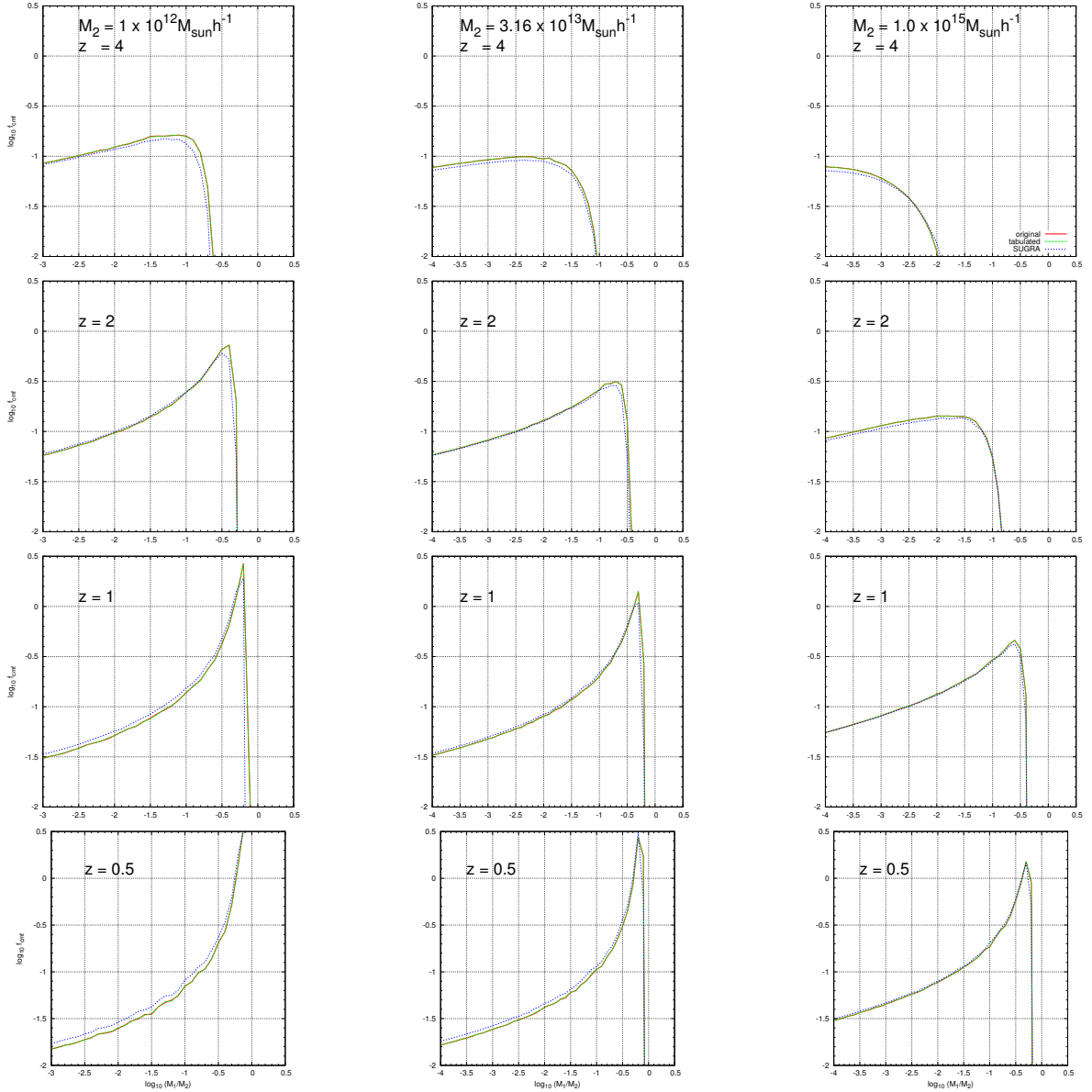
Figure 10: The conditional mass functions for 10000 halos evenly distributed around mass M_2 with a factor of $\sqrt{2}$ on each side for given redshifts. This is quite similar to figure 1 in Parkinson et al. (2008). It goes further towards small masses on the left hand side because the resultion of our halo was much bigger. 'Tabulated' and 'Original' are MS cosmologies, to see if our adapted code reproduces the original code in the limiting case of a ΛCDM cosmology. The other cosmology plotted is a SUGRA case, since we had a simulation for this cosmology at our disposal to check the modified MERGER-TREES code against an N-body simulation.)
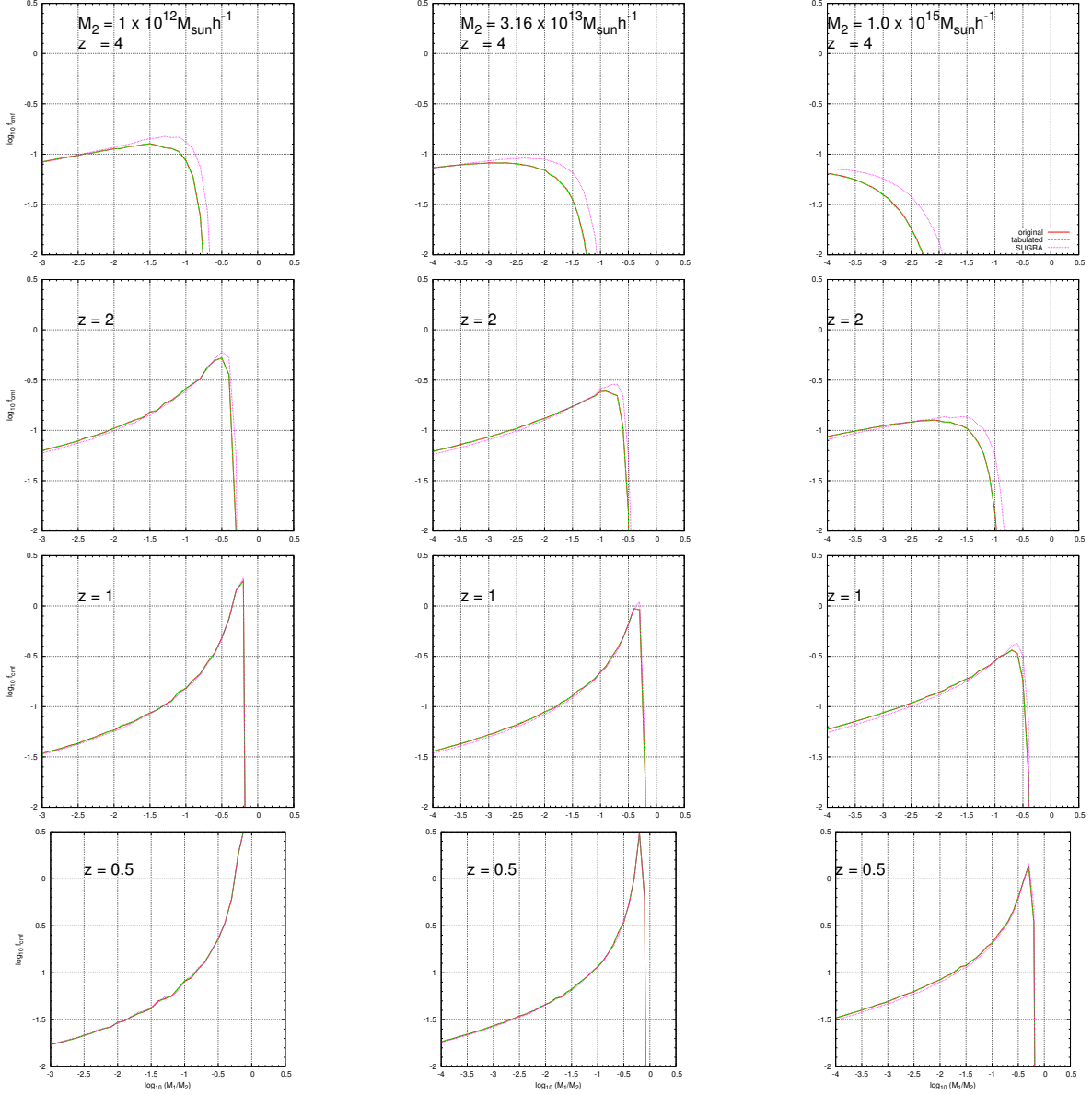
Figure 11: The conditional mass functions for 10000 halos evenly distributed around mass M_2 with a factor of $\sqrt{2}$ on each side for given redshifts. The ΛCDM-case here is 'Sanchez'. In this verison, we can see clearly that there are differences arising at redshifts $z \sim 2$. This is due to the different expansion histories of the cosmolgies and could possibily be detectable in the galaxy population, if GALFORM is run on these cosmologies. The differences seem also greater for bigger base masses M_2.
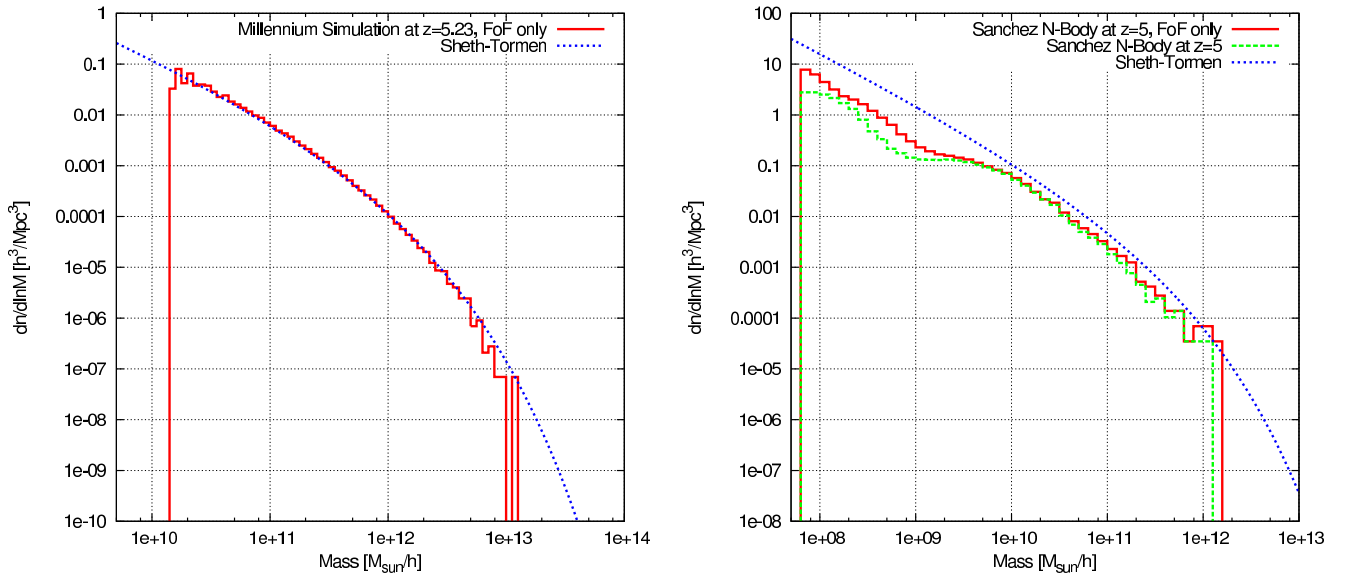
Figure 12: Left panel: The mass function extracted from the MS using our code. It fits nicely to the analytical mass function of Sheth & Tormen (2002). To calculate this, we have used the according module of the 'Cosmology Routine Library' maintained by E. Komatsu (`http://www.mpa-garching.mpg.de/~komatsu/CRL/`).
Right panel: The odd mass function of the 'Sanchez' simulation. Both the FoF output and the post-SUBFIND output are shown, both have the same features. Thus, our code (which is implemented post-SUBFIND) is not causing this. Something has gone awry, there are many objects missing on the low mass scale, and the function, although lining up with the analytical curve, never quite touches it. The same is the case for the SUGRA simulation.

4. Results

The results are clearly encouraging. The implementation of a monte-carlo algorithm that takes different cosmologies has been completed. We still need to check its viability against N-body simulations, which have been provided but were shown to be faulty. So the code still needs to be verified, which requires at least 2 well-resolved N-body simulations. In the case of ΛCDM, the altered code reproduces the original's results very well.

Part of the extended MERGER-TREES is now a script that computes δ_{crit} for the different cosmologies presented in this work. This can easily be appended to other cosmologies, if the function $w(a)$ is specified.

In the whole process, a variety of code was written to read out and analyse output from MERGER-TREES, which will be useful for future studies with this algorithm. Furthermore, a little library called `mt_functions` for functions that are useful in this context (i.e. reading out data from monte-carlo and N-body simulations, generating mass functions for N-bodys at given snapshot, generating conditional mass functions for both, ...) was put together, see A.2.

Currently, the author is looking at ways to parallelise these codes, in order to make use of the now standard multi-core processors more effectively.

The different models give different growth functions (fig. 1), different power spectra (fig. 9), and different $\delta_{crit}(a)$ (fig. 8). This leads to a divergence in the conditional mass functions (see fig. 11), which, in turn, should affect galaxy formation quite drastically, especially at high redshift. This is, however, subject to future work, due to the limited time frame available in this project work.

5. Conclusions & Future work

5.1. On the Simulations

As stated before, the next step would be to find out what went wrong with the simulations. It is likely due to the chosen initial conditions. However, we need to get into contact with the person who ran the simulations to confirm what exactly has been done. Maybe running an own set of N-body simulations is less time-consuming and more fruitful.

If we then obtain sensible output, we can compare the output of MERGER-TREES to the new N-body simulations, and see whether the implementation of the new cosmologies was successful. If it is not, maybe the parameters presented with the 'New Tree' corrections by Parkinson et al. (2008) have to be revised.

5.2. Running Galform

If the output of the algorithm matches the simulations well enough, we can comfortably (and quickly!) generate merger trees for our different cosmologies. Running GALFORM on those then will give us numerous observables, such as the luminosity function, galaxy counts, SFR, etc. This can then finally be compared to large surveys such as SDSS or GAMA. This will be a novel piece of information. By looking at extremes, maybe we can rule out models (i.e. if we find older galaxies in our universe than one model predicts).

Do we maybe have to tweak the parameters of GALFORM very strongly to reproduce observed galaxy properties? Can we perhaps rule out a model from requiring unrealistic points in parameter space to fit observations?

There is clearly a lot of exciting work ahead if the modified MERGER-TREES code proves to be consistent with different cosmologies. Obviously, the ultimative test of all physics is always observation of nature. If a theory doesn't agree with observations, it is advisable to find something that does, until the observations (or the experiments, to not be branch-specific) get more precise or more general. Therefore, we should find a recent catalogue that has enough high-z galaxies to compare it to our models.

5.3. Final conclusions

To sum up, this project is well underway of at least delivering the answers to the question whether the current version of MERGER–TREES is compatible with different Dark Energy cosmologies. If it is, we have a lot of work ahead to establish how Dark Energy can affect galaxy formation. Global galaxy properties can then perhaps established as novel Dark Energy observable.

If we can not establish MERGER–TREES' compatibility to different cosmologies, maybe a further

correction in the style of Parkinson et al. (2008) can solve this problem and generalise the code further.

Acknowledgements

The author owes thanks to Carlton Baugh especially for taking him on, even on such short notice and trusting him with such an exciting project. Also, John Helly was very supportive with his continuing help with MPI and the gadget read-out process, providing some of his own code. Thanks to Lydia Heck for a quick and uncomplicated setup of an account on cosma and lightning-quick support email replies.

The author would very much like to continue with this work and see where it leads.

References

Amendola L., Tsujikawa S., 2010, Dark Energy: Theory and Observations, in press 07/2010 edn. Cambridge University Press

Baugh C. M., Lacey C. G., Frenk C. S., Granato G. L., Silva L., Bressan A., Benson A. J., Cole S., 2005, MNRAS, 356, 1191

Bennett C. L., Bay M., Halpern M., Hinshaw G., Jackson C., Jarosik N., Kogut A., Limon M., Meyer S. S., Page L., Spergel D. N., Tucker G. S., Wilkinson D. T., Wollack E., Wright E. L., 2003, The Astrophysical Journal, 583, 1

Benson A. J., Bower R. G., Frenk C. S., Lacey C. G., Baugh C. M., Cole S., 2003, Astrophys.J., 599, 38

Benson A. J., Lacey C. G., Baugh C. M., Cole S., Frenk C. S., 2002, MNRAS, 333, 156

Boggess N. W., Mather J. C., Weiss R., Bennett C. L., Cheng E. S., Dwek E., Gulkis S., Hauser M. G., Janssen M. A., Kelsall T., Meyer S. S., Moseley S. H., Murdock T. L., Shafer R. A., Silverberg R. F., Smoot G. F., Wilkinson D. T., Wright E. L., 1992, Astrophys. J., 397, 420

Cole S., Helly J., Frenk C. S., Parkinson H., 2008, Mon.Not.Roy.Astron.Soc., 383, 546

Cole S., Lacey C. G., Baugh C. M., Frenk C. S., 2000, MNRAS, 319, 168

Corasaniti P. S., Copeland E. J., 2003, Phys. Rev. D, 67, 063521

Dicke R. H., Peebles P. J. E., Roll P. G., Wilkinson D. T., 1965, Astrophys. J., 142, 414

Dodelson S., 2003, Modern cosmology. Academic Press, Amsterdam [u.a.], pp. XIII, 440 S., includes bibliographical references and index

Einstein A., 1917, in Sitzungsberichte der Königlich-Preußischen Akademie der Wissenschaften, pp. 142–152

Fang W., Hu W., Lewis A., 2008, Phys.Rev., D78, 087303

Guth A. H., 1981, Phys. Rev. D, 23, 347

Jennings E., Baugh C. M., Angulo R. E., Pascoli S., 2010, Mon.Not.Roy.Astron.Soc., 401, 2181

Komatsu E., Dunkley J., Nolta M. R., Bennett C. L., Gold B., Hinshaw G., Jarosik N., Larson D., Limon M., Page L., Spergel D. N., Halpern M., Hill R. S., Kogut A., Meyer S. S., Tucker G. S., Weiland J. L., Wollack E., Wright E. L., 2009, Astrophys.J.Suppl., 180, 330

Komatsu E., Smith K. M., Dunkley J., Bennett C. L., Gold B., Hinshaw G., Jarosik N., Larson D., Nolta M. R., Page L., Spergel D. N., Halpern M., Hill R. S., Kogut A., Limon M., Meyer S. S., Odegard N., Tucker G. S., Weiland J. L., Wollack E., Wright E. L., 2011, Astrophys.J.Suppl., 192, 18

Lewis A., Challinor A., Lasenby A., 2000, Astrophys. J., 538, 473

Linder E. V., Jenkins A., 2003, MNRAS, 346, 573

Maor I., Lahav O., 2005, 7, 3

Pace F., Waizmann J.-C., Bartelmann M., 2010, Mon.Not.Roy.Astron.Soc., 406, 1865

Parkinson H., Cole S., Helly J., 2008, Mon.Not.Roy.Astron.Soc., 383, 557

Penzias A. A., Wilson R. W., 1965, Astrophys. J., 142, 419

Planck Science Team, 1996, Redbook

—, 2012, Planck's HFI completes its survey of early Universe.
  News retrieved from www.esa.int on 16/01/12

Press W. H., Schechter P., 1974, Astrophys.J., 187, 425

Reid B. A., et al., 2010, Mon.Not.Roy.Astron.Soc., 401, 2148

Riess A. G., Macri L., Casertano S., Sosey M., Lampeitl H., et al., 2009, Astrophys.J., 699, 539

Sánchez A. G., Crocce M., Cabré A., Baugh C. M., Gaztañaga E., 2009, MNRAS, 400, 1643

Sheth R. K., Tormen G., 2002, MNRAS, 329, 61

Springel V., White S. D. M., Tormen G., Kauffmann G., 2001, MNRAS, 328, 726

Wang J., De Lucia G., Kitzbichler M. G., White S. D., 2007, Mon.Not.Roy.Astron.Soc.

A. Appendix

A.1. WMAP 7 data

WMAP Cosmological Parameters			
Model: wcdm+sz+lens			
Data: wmap7+bao+h0			
$10^2\Omega_b h^2$	2.246 ± 0.058	$1 - n_s$	$0.041^{+0.015}_{-0.014}$
$1 - n_s$	$0.012 < 1 - n_s < 0.068$ (95% CL)	$1 + w$	-0.10 ± 0.14
$1 + w$	$-0.39 < 1 + w < 0.15$ (95% CL)	$A_{\mathrm{BAO}}(z = 0.35)$	0.471 ± 0.012
C_{220}	5755 ± 40	$d_A(z_{\mathrm{eq}})$	14188 ± 144 Mpc
$d_A(z_*)$	14022 ± 146 Mpc	$\Delta_{\mathcal{R}}^2$	$(2.49 \pm 0.12) \times 10^{-9}$
h	$0.720^{+0.027}_{-0.028}$	H_0	$72.0^{+2.7}_{-2.8}$ km/s/Mpc
k_{eq}	$0.01004^{+0.00038}_{-0.00037}$	ℓ_{eq}	140.7 ± 4.0
ℓ_*	$302.54^{+0.78}_{-0.79}$	n_s	$0.959^{+0.014}_{-0.015}$
Ω_b	$0.0435^{+0.0036}_{-0.0037}$	$\Omega_b h^2$	0.02246 ± 0.00058
Ω_c	$0.222^{+0.015}_{-0.016}$	$\Omega_c h^2$	$0.1150^{+0.0053}_{-0.0052}$
Ω_Λ	$0.734^{+0.019}_{-0.018}$	Ω_m	$0.266^{+0.018}_{-0.019}$
$\Omega_m h^2$	$0.1374^{+0.0052}_{-0.0051}$	$r_{\mathrm{hor}}(z_{\mathrm{dec}})$	$283.3^{+2.7}_{-2.8}$ Mpc
$r_s(z_d)$	152.1 ± 1.5 Mpc	$r_s(z_d)/D_v(z = 0.2)$	$0.1914^{+0.0043}_{-0.0042}$
$r_s(z_d)/D_v(z = 0.35)$	0.1142 ± 0.0021	$r_s(z_*)$	145.6 ± 1.4 Mpc
R	1.733 ± 0.018	σ_8	0.846 ± 0.059
A_{SZ}	$0.92^{+0.69}_{-0.92}$	t_0	13.74 ± 0.11 Gyr
τ	0.086 ± 0.014	θ_*	0.010384 ± 0.000027
θ_*	0.5950 ± 0.0015 °	t_*	375369^{+4704}_{-4792} yr
w	-1.10 ± 0.14	z_{dec}	1088.5 ± 1.2
z_d	$1020.4^{+1.3}_{-1.4}$	z_{eq}	3292^{+125}_{-123}
z_{reion}	$10.4^{+1.1}_{-1.2}$	z_*	$1091.31^{+0.98}_{-0.97}$

Table 3: Cosmological parameter table taken from (**?**); its underlying model is WCDM, meaning that the Dark Energy equation of state is allowed to vary in time and that the dark matter is cold (i.e. $T \ll m$). The precision is of the parameters is remarkable, given their great number, even if there are degeneracies here and there. The WMAP data is complemented by BAO (baryo-accoustic oscillations, the remnants of the fact that the baryons followed the photons' oscillations before decoupling) (Reid et al., 2010) and H_0 from Hubble Space Telescope (HST) observations (Riess et al., 2009).

A.2. Python source code

Since the original idea of printing the code with the report was quite wasteful, digital copies of the code can be found here: `http://tinyurl.com/mergertrees-code`

A.3. Linear density field evolution

Let's ask ourselves how the fluids are behaving given a specific background cosmology. On the linear level, this can be solved analytically, as we will see in this section. However, most of the interesting physics is going on during the highly nonlinear periods. This is where numerical solutions, computer simulations and semi–analytical models have to be considered.

The basis for this is perturbation theory. The first step is perturbing the background metric by a small amount $\delta g_{\mu\nu}$:

$$g_{\mu\nu} = g_{\mu\nu}^{(0)} + \delta g_{\mu\nu} \tag{A.1}$$

The perturbed metric is usually depicted thusly:

$$\delta g_{\mu\nu} = a^2 \begin{pmatrix} -2\Psi & w_i \\ w_i & 2\Phi\delta_{ij} + h_{ij} \end{pmatrix} \tag{A.2}$$

Note that w_i here is an arbitrary 3-vector, and has nothing to do with the equation of state.

From there, symmetry arguments, Helmholtz' theorem and gauge choice leads to this line element (see e.g. (Amendola & Tsujikawa, 2010) or most standard cosmology textbooks for a detailed derivation):

$$ds^2 = (-1 - 2\Psi)dt^2 + a^2(1 + 2\Phi)\delta_{ij}dx^i dx^j \tag{A.3}$$

Then, by plugging this into Einstein's field equations, only keeping terms of first order in δ and assuming the energy–stress–tensor to be that of a perfect fluid, one arrives at a set of equations, for simplicity usually written in Fourier space, which can be combined to yield the relativistic Poisson equation,

$$k^2\Phi = 4\pi G a^2 \rho[\delta + 3\mathcal{H}(w+1)\frac{\theta}{k^2}], \tag{A.4}$$

a differential equation for the gravitational potential Φ (which is related to Ψ via $\Phi = -\Psi$ iff $T_{\mu\nu}$ is shearless, i.e. $T_{ij} = 0$. This is true for (cold) Dark Matter and standard Dark Energy.),

$$\Phi'' + 3\mathcal{H}(1 + c_s^2)\Phi' + (c_s^2 k^2 + 3\mathcal{H}^2 c_s^2 + 2\mathcal{H}' + \mathcal{H}^2)\Phi = 0, \tag{A.5}$$

where the density contrast $\delta := (\rho(x,t) - \rho_0)/\rho_0$, the velocity divergence $\theta := \partial_i v^i$, the conformal Hubble function $\mathcal{H} := aH$ and the soundspeed $c_s^2 = \frac{dP}{d\rho}$. Note that a prime denotes a derivative w.r.t. conformal time η[¶] The former two equations can be combined into one handy equation for the 'total-matter variable' $\tilde{\delta} := \delta + 3\mathcal{H}(w+1)\theta/k^2$:

$$\tilde{\delta}'' + \mathcal{H}(1 + 3c_s^2 - 6w)\tilde{\delta}' - \left(\frac{3\mathcal{H}^2}{2}(1 - 6c_s^2 - 3w^2 + 8w) - c_s^2 k^2\right)\tilde{\delta} = 0 \tag{A.6}$$

This equation can now be specified for different kinds of fluid. If we're looking at scales much smaller than the Hubble radius (i.e. $k \gg \mathcal{H}$), and restrict ourselves to a pressureless fluid with small sound

---

[¶]Conformal time: $\eta(t) = \int_0^t a^{-1}dt'$

speed (i.e. cold dark matter, or decoupled baryons), the former equation reduces to

$$\delta'' + \mathcal{H}\delta' + \left(c_s^2 k^2 \delta - \frac{3}{2}\mathcal{H} \right) \delta = 0, \tag{A.7}$$

which is basically a fluid wave with Hubble friction.

For $c_s k \ll \mathcal{H}$ (again, CDM or decoupled baryons), this becomes

$$\delta'' + \mathcal{H}\delta' - \frac{3}{2}\mathcal{H}^2 \delta = 0, \tag{A.8}$$

which can be neatly re-written if we take derivatives w.r.t. $d\ln a$ instead of $d\eta$:

$$\frac{d^2}{d\ln a^2}\delta + \frac{1}{2}\frac{d}{d\ln a}\delta - \frac{3}{2}\delta = 0. \tag{A.9}$$

The two analytic solutions to this are

$$\delta_+ = Aa \quad \delta_- = Ba^{-3/2} \tag{A.10}$$

A and B are fixed by boundary conditions. Here, subscript '+' denotes a *growing* solution, and '-' a *decaying* one. The former is the more interesting one if we're looking for gravitational instabilities that form the seeds for galaxy formation. This solution, dubbed the growth function $D(a)$, is $\propto a$ in a matter–dominated universe. It will be $< a$ if something else, such as Dark Energy takes over and accelerates the Hubble expansion faster than the gravitational potential Φ grows. Again, for a more detailed treatment of the matter, the reader is referred to their favourite cosmology textbook.

A.4. The matter power spectrum

The importance of the power spectrum to cosmology cannot be overstated. It is a statistical measure of correlation in k-space and does not evolve during linear structure growth, since in this regime, the gravitational potential (and therefore the density contrast) can be seperated according to

$$\Phi(k, a) = 0.9\Phi(k, a_{initial})T(k)D(a). \tag{A.11}$$

To show that this seperation is valid is a nontrivial exercise, as said before, most textbooks cover it or refer to a proof (e.g. Amendola & Tsujikawa (2010) or Dodelson (2003)).

The power spectrum is defined by

$$P(\mathbf{k}) = V^{-1} \int dV_x dV_y \; \delta(\mathbf{x})\delta(\mathbf{y})e^{-i\mathbf{k}\cdot(\mathbf{x}-\mathbf{y})}, \tag{A.12}$$

where $\delta(\mathbf{x})\delta(\mathbf{y}) = \xi(\mathbf{x} - \mathbf{y}) = \xi(\mathbf{r})$ is the 2-point (or auto-) *correlation function*. In general, there is an n-point correlation function; for a gaussian distribution, all odd moments (i.e. $2n + 1$-correlation functions) disappear.

Another parameter that quantifies the clustering property of a universe is the root mean square fluctuations in a given scale R, called σ_R.

For a sphere of radius R, this is defined by

$$\sigma_R^2 = (2\pi^2)^{-1} \int dk \; P(k) W_R^2(k) k^2.$$ (A.13)

The window function W_R is a top hat in real space, cutting off all contributions $> R$. In k-space it has oscillatory features. The the prefactor and the factor of k^2 are due to the spherical symmetry, and $P(k)$, as stated before, quantifies the fluctuations. Usually R is taken to be 8Mpc/h, which is more of a 'historic relic' than a conscious choice.